Thermographic measurement of the emittance plot of a single positive ion beamlet

M. Kovari,[a] B. Crowley, and S. J. Cox[b]
UKAEA/Euratom Fusion Association, Culham Science Centre, Abingdon, Oxon OX14 3DB, United Kingdom

(Received 12 February 2008; accepted 22 March 2008; published online 14 April 2008)

Measurements have been made of the emittance plot of a partly neutralized positive ion beamlet, using a slit, a polymer target, and an infrared camera. This thermographic approach is intrinsically linear and absolute (since the properties of the target are known and approximately independent of temperature). It is sufficiently sensitive that only one short pulse is required to capture the entire range of the angular coordinate y'. Ions and neutral atoms are both detected with equal sensitivity. The measurement is unaffected by secondary electrons emitted by the target and by electrons traveling with the positive ion beam, as both types of electron carry very little energy. No specialized electronics or beam deflection devices are required. Providing the region downstream of the mask is free of fields, the target can be several meters away from the mask, allowing good resolution in the y' axis. The target can be as large as required. © *2008 American Institute of Physics.* [DOI: 10.1063/1.2908164]

The *emittance plot* of a particle beam is the distribution of particle density in the xx' or yy' plane, where z is the beam axis, $x'=dx/dz$, and $y'=dy/dz$.[1] It provides much more information than the *emittance*—a numerical quantity defined in terms of the area occupied in the emittance plot. In principle, the plot can also be projected forward or backward to determine the size and shape of the beam at any given plane.

While most work has used electrical detectors to determine the emittance plot,[2] using the principle illustrated in Fig. 1, other detection methods have also been used. Various light emitting screens have been used,[3] including Ce:YAG,[4] and Al_2O_3.[5] Guharay *et al.*[6] used a 50 μm Kapton film. The Kapton becomes darker with exposure to the beam. After a large number of identical shots, the target is removed from the vessel and its transparency is measured.

This paper describes measurements of the emittance plot of a partly neutralized D^+ beam, using a slit, a polymer target, and an infrared camera. The benefits of this approach are described in the abstract above.

The beam was produced by a tetrode accelerator with a standard JET ion source. The hole diameters in grids 1 (plasma grid) to 4 (grounded grid) were 12, 13, 10, and 12 mm, respectively. The grid spacings are shown in Fig. 2(a). The JET ion source with an accelerator is known as a "PINI."[7]

All but one of the 262 holes in the plasma grid were blocked with copper plugs. A molybdenum mask was fixed in position immediately downstream of the neutralizer. The mask had a recessed slit [Fig. 2(b)] and an array of recessed holes of nominal diameter 0.2 mm. The final breakthrough of the holes and slit was done by laser machining.[8]

As the mask could not be moved, the PINI was steered up or down in steps to scan the beamlet over the slit, with one pulse taken at each position. For each pulse, a series of infrared images were taken of the target, using an infrared camera.[9]

A small portion of the beamlet passed over the top of the mask. The overspill image on the target was hotter than the slit image, but sufficiently separated from it to allow the slit image to be analyzed. The amount of energy passing through the array of holes was not sufficient for the IR camera to produce a usable image.

A thermal model of the mask showed that thermal distortion greatly reduces the slit width if the pulse length is ~100 ms. If the parallel-sided recess was replaced by a V-shaped chamfer, this problem would be greatly reduced. Note that in either case the recess or chamfer should be on the upstream side. This is the opposite of the approach normally used to prevent scattering. The recess used was wide enough that any scattered particles will land well away from the target.

The target was Kapton XC, 40 μm thick. This is a black, carbon-loaded, electrically conductive polyimide, thermally durable to 325 °C in oxygen-free environments.[10] The carbon is present throughout the bulk of the film, so it cannot rub or flake off. Non-loaded Kapton is translucent, both in the visible and infrared. The carbon makes the film opaque and prevents charging from the beam.

The timescale for heat to spread through the thickness of the target is of the order of (target thickness)^2/thermal diffusivity=0.02 s. The thermal images used for analysis

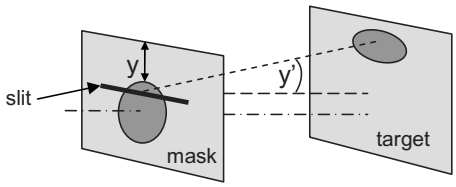

FIG. 1. The principle of measurement of the emittance plot.

[a]Electronic mail: michael.kovari@jet.uk.
[b]Deceased.

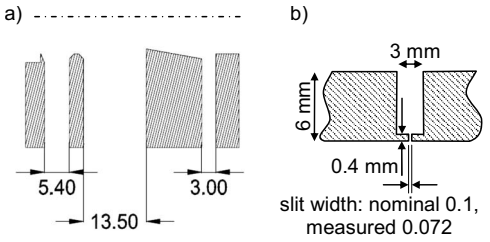

FIG. 2. (a) Cross section of grid, with half of the aperture. (b) Cross section of slit in mask. Dimensions in mm.

were taken about 50 ms after the end of the pulse, long enough for the temperature to be uniform through the thickness of the target, but short enough that very little heat spreads transversely.

The emissivity of Kapton XC was measured in air. Linear fits to the emissivity are $0.95-0.0007\Theta$ and $0.94-0.0005\Theta$ for the matt and shiny sides, respectively, where Θ is the temperature in °C.

The last image before the pulse was subtracted from the image taken about 50 ms after the end of the pulse, giving a temperature change image (Fig. 3). A set of lines was drawn on the image, parallel to each other and to the axis of the slit image. The mean temperature rise along each line was calculated. Each pulse corresponds to one value of y. Each line corresponds to one value of y'.

The differential power at the mask is given by

$$\frac{d^2P}{dydy'} = \Delta T \frac{c\rho d}{t} \cdot \frac{Ld_{mt}}{\delta}, \tag{1}$$

where P is the power at the mask, y and y' are shown in Fig. 1, ΔT is the temperature rise of the target, averaged along a line of length L, c is the specific heat capacity of the target, ρ is the density of the target, d is the thickness of the target, t is the pulse length, d_{mt} is the distance from mask to target, and δ is the width of the slit in the mask.

The emittance plot shows $d^2P/dydy'$ against y and y'. These measurements give the emittance plot at the mask. Assuming the region is field-free, the emittance plot at any other plane can be calculated.

The emittance diagram is most usefully plotted at grid 4, since beam simulations are likely to end there. Consequently,

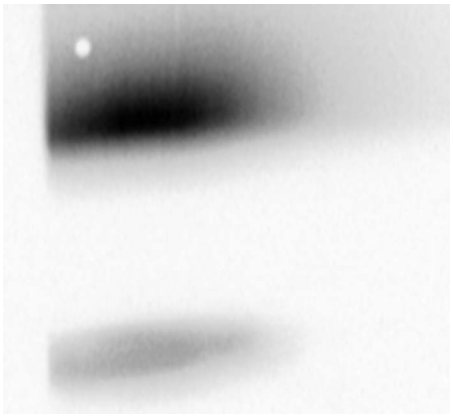

FIG. 3. Typical infrared image, showing overspill (top) and slit image (bottom).

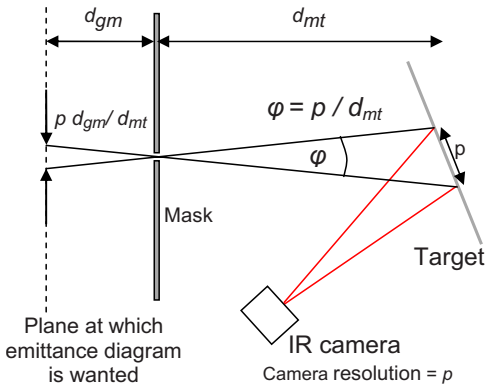

FIG. 4. (Color online) The effect of the resolution of the IR camera.

it is important to estimate the achievable spatial and angular resolutions at grid 4.

Figure 4 illustrates the effect that the finite spatial resolution of the IR camera has on the resolution of the emittance plot at grid 4. The two lines represent extreme particle paths that land on points of the target that are too close to be distinguished. The angle between the paths represents the angular resolution, and the separation of the paths at grid 4 represents the spatial resolution. Figure 5 illustrates the effects of slit width. The two lines represent extreme particle paths that cannot be distinguished because they land in the same place on the target.

Combining these two effects, the net spatial resolution Δy at grid 4 is

$$\Delta y = \sqrt{\left(\delta \cdot \frac{d_{mt} + d_{gm}}{d_{mt}}\right)^2 + \left(p\frac{d_{gm}}{d_{mt}}\right)^2}, \tag{2}$$

and the angular resolution $\Delta y'$ is

$$\Delta y' = \sqrt{\left(\frac{\delta}{d_{mt}}\right)^2 + \left(\frac{p}{d_{mt}}\right)^2}, \tag{3}$$

where p is the spatial resolution of the IR camera at the target, d_{gm} is the distance from grid 4 to mask, and d_{mt} and δ are defined above.

These formulas need to be modified if the target is not normal to the beam. Estimates using these formulas are $\Delta y = 0.8$ mm and $\Delta y' = 0.4$ mrad, but it is not possible to confirm these by using the measured results. The beam was not scanned over the slit in small enough steps to cover the emittance plot in sufficient detail.

When using an array of holes, the diameter of the image of a pinhole must be calculated to ensure that the separate pinhole images do not overlap. The geometrical image of the aperture in grid 4 is the upper limit. The angular spread of

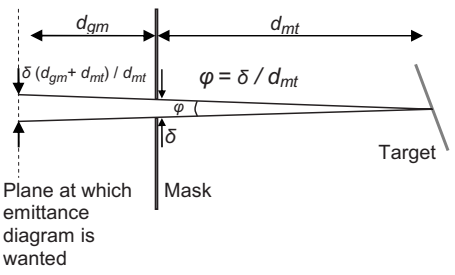

FIG. 5. The effect of slit width.

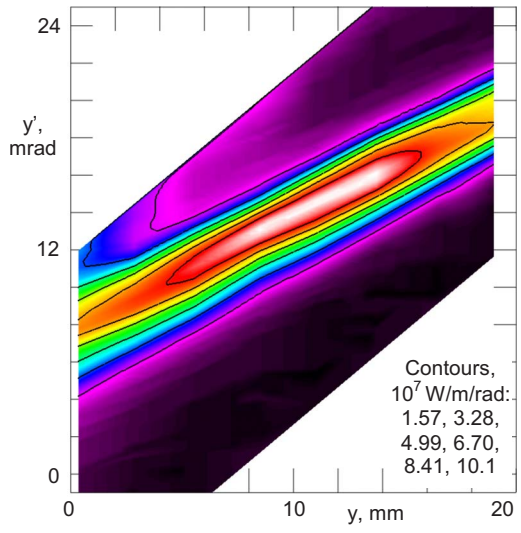

FIG. 6. (Color online) Emittance plot at mask, 108 kV, pulse length of 37 ms, 122 mA.

the beamlet determines whether this image is fully illuminated. Consequently, the image on the target of a pinhole on the beamlet axis is given by the smaller of the two quantities,

$$a = \phi_{\text{beamlet}} \cdot \frac{d_{mt}}{d_{gm}}$$

and

$$b = \theta_c \cdot d_{mt}, \tag{4}$$

where ϕ_{beamlet} is the diameter of the beamlet at grid 4 and θ_c is the maximum angle of convergence of the particles reaching the mask. (Whether this is the same as the overall beamlet divergence angle depends on the shape of the emittance plot.)

The emittance plots at the mask and extrapolated to grid 4 are shown in Fig. 6. The origins of the y and y' scales are arbitrary. It is not possible to calculate the emittance, as much of the emittance plot is missing because it was not possible to scan the beamlet sufficiently far up or down.

In conclusion, the thermography technique for measurement of emittance plots was successful, but in the angular coordinate (y') measured at grid 4 the sampling interval was too large and the extent of coverage was insufficient. Several improvements are suggested.

(1) The mask should be bigger to prevent overspill.
(2) The slit should be chamfered rather than recessed to minimize thermal distortion.
(3) The mask should be as close as possible to the accelerator to improve resolution in y. To ensure adequate sampling, the mask must be stepped in fractions of a millimeter, right out to the edge of the beam.
(4) An aperture with no offset aperture steering should be used to guarantee symmetry. A second aperture with steering, well separated from the first, could be used for comparison.

This work is dedicated to our colleague S.J.C. whose tragic death occurred while this work was in progress. M. K. and B. C. would like to thank F. Long, M. Barnard, R. Robins, and T. Jones. This work has been conducted under the European Fusion Development Agreement and is funded partly by EURATOM and by the UK Engineering and Physical Science Research Council.

[1] J. D. Lawson, *The Physics of Charged-Particle Beams*, 2nd ed. (Clarendon, New York, 1988).
[2] C. Lejeune and J. Aubert, Adv. Electron. Electron Phys., Suppl. **13A**, 159 (1980).
[3] J. G. Wang, D. X. Wang, and M. Reiser, Nucl. Instrum. Methods Phys. Res. A **A307**, 190 (1991).
[4] L. Catani, E. Chiadroni, A. Cianchi, S. Tazzari, M. Boscolo, M. Castellano, G. Di Pirro, M. Farrario, V. Fusco, D. Filipetto, L. Palumbo, C. Vaccarezza, C. Vicario, and C. Ronsivalle, Rev. Sci. Instrum. **77**, 093301 (2006).
[5] T. Hoffmann, W. Barth, P. Forck, A. Peters, P. Strehl, and D. A. Liakin, AIP Conf. Proc. **546**, 432 (2000).
[6] S. K. Guharay, K. Tsumori, M. Hamabe, Y. Takeiri, O. Kaneko, and T. Kuroda, Rev. Sci. Instrum. **67**, 2534 (1996).
[7] G. Duesing, H. Altmann, H. Falter, A. Goede, R. Haange, R. S. Hemsworth, P. Kupschus, D. Stork, and E. Thompson, Fusion Technol. **11**, 163 (1987).
[8] UK Laser Micromachining Centre, www.uk-lmc.co.uk.
[9] Agema Thermovision 550, FLIR Systems, +44(0)1732-220-011, www.flir.com.
[10] www2.dupont.com.